



intensity on a silicon substrate, due to non-radiative processes. Surprisingly, at smaller separations we observe reduced quenching of QD emission on MoS<sub>2</sub>, despite the presence of significant non-radiative charge transfer. Interestingly, at small separations  $\delta$ , we see evidence of strong dot-dot interactions and a significant red shift of QD PL spectral maxima which enhances spectral overlap with the absorption of B excitons of MoS<sub>2</sub>. However, instead of increased probability of non-radiative resonant energy transfer to MoS<sub>2</sub> from QDs and strong quenching of QD photoluminescence (PL), due to the enhanced spectral overlap, we find considerable reduction in the quenching of the PL of QDs compared to that expected from standard non-radiative processes. Significantly we observe that simultaneously the intensity of the B exciton of MoS<sub>2</sub> increases significantly suggesting the possibility of coherent and resonant radiative energy exchange between the 0D excitons in QDs and the 2D B exciton in MoS<sub>2</sub>. Our study reveals interesting nanoscale light-matter interaction effects which can suppress the conventional quenching of QDs leading to potential applications of these nanoscale devices in light emitting and photonic devices.

## 2 Experimental details

MoS<sub>2</sub> monolayers were exfoliated on polydimethylsiloxane (PDMS) sheets and then transferred onto 300 nm SiO<sub>2</sub> substrates. Monolayers were confirmed through optical and Raman spectroscopy. QDs were synthesized following methods described earlier.<sup>16,17</sup> The monolayer of QDs was transferred onto MoS<sub>2</sub> using the Langmuir-Blodgett (LB) technique.<sup>18,19</sup> QDs in chloroform were spread on a deionized (DI) water-filled LB trough (Kibron Microtrough G2, Finland) to get a monolayer and the monolayer was slowly transferred onto the substrate at constant surface pressure. The ligand exchange was done by slightly modifying an earlier<sup>20</sup> report (ESI<sup>†</sup>). In a typical ligand exchange, the vapor of K<sub>2</sub>S in formamide solution was exposed to the QD-MoS<sub>2</sub> sample overnight and the excess ligand was washed with toluene and formamide solution, and using this

method we exchanged the TOPO (long) ligand with the sulfur (short) ligand.

Atomic force microscopy was performed using a Park system (NX model) in non-contact mode. PL spectra were collected using a Horiba (LabRam model) instrument, using a 532 nm continuous wave (CW) laser. A laser power of  $\sim 1 \mu\text{W}$  was used to avoid the bleaching of QDs. Signals were collected using a charge coupled device (CCD). A 300 g mm<sup>-1</sup> grating and 1800 g mm<sup>-1</sup> grating were used to collect the PL and the Raman spectra respectively. Time resolved PL (TRPL) data were collected using a PicoQuant MicroTime 200 system, with a temporal resolution of 25 ps. A 507 nm laser with 40 MHz repetition rate was used to excite the sample keeping the power at  $\sim 1 \mu\text{W}$ . A band pass filter was used to collect QD TRPL spectra. A 50 $\times$  (Olympus NA-0.45) objective was used to collect both PL and TRPL data.

## 3 Results and discussion

Fig. 1 shows the schematic of how the ligand exchange affects the separation (coupling) between the QD-MoS<sub>2</sub> hetero-structure. The ligand exchange not only decreases the separation  $d$  between the QDs and MoS<sub>2</sub> but also decreases the separation between the QDs  $\delta$  themselves. When the long TOPO capped ligand is attached to QDs the  $d$  is  $\sim 2$  nm, and the  $\delta$  is  $\sim 4$  nm. After ligand exchange these separations decrease to  $\sim 0.3$  nm and  $\sim 0.6$  nm respectively.

Fig. 2(a) shows the optical image of MoS<sub>2</sub> before the transfer of monolayer QDs. Fig. 2(b) shows the optical images of the MoS<sub>2</sub>-QD hetero-structure after transferring the monolayer of the QD film using the LB technique. The QD monolayer is transferred uniformly onto the MoS<sub>2</sub> layer. Fig. 2(c) shows the isotherm (surface pressure vs. area plot) of LB transfer; the QD monolayer was transferred at a surface pressure of 35 mN m<sup>-1</sup>. The 0D-2D hetero-structures were further characterized using atomic force microscopy (AFM). Fig. 2(d) shows the Raman spectra of MoS<sub>2</sub> and the MoS<sub>2</sub>-QD hetero-structure before and after ligand exchange. The A<sub>1g</sub> mode is slightly affected after transferring the QD layer.

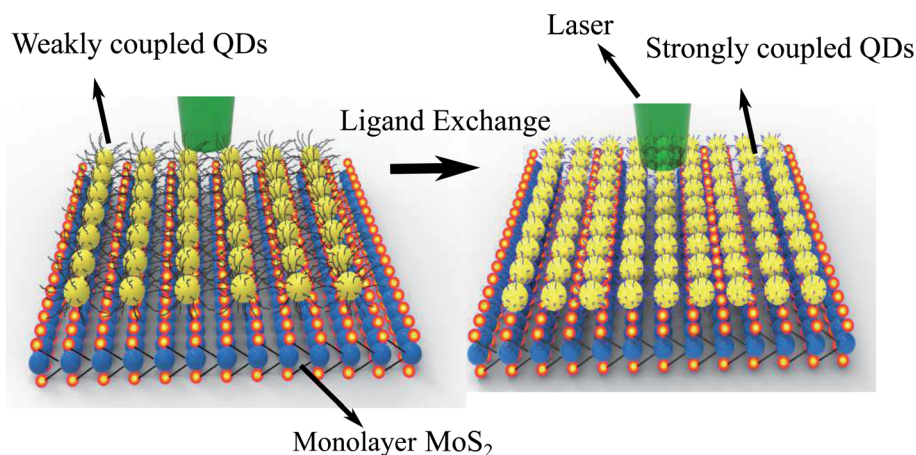


Fig. 1 The schematic of how the ligand exchange treatment affects the separation between the QD-MoS<sub>2</sub> hetero-structure; this treatment also modifies the dot-dot separation.



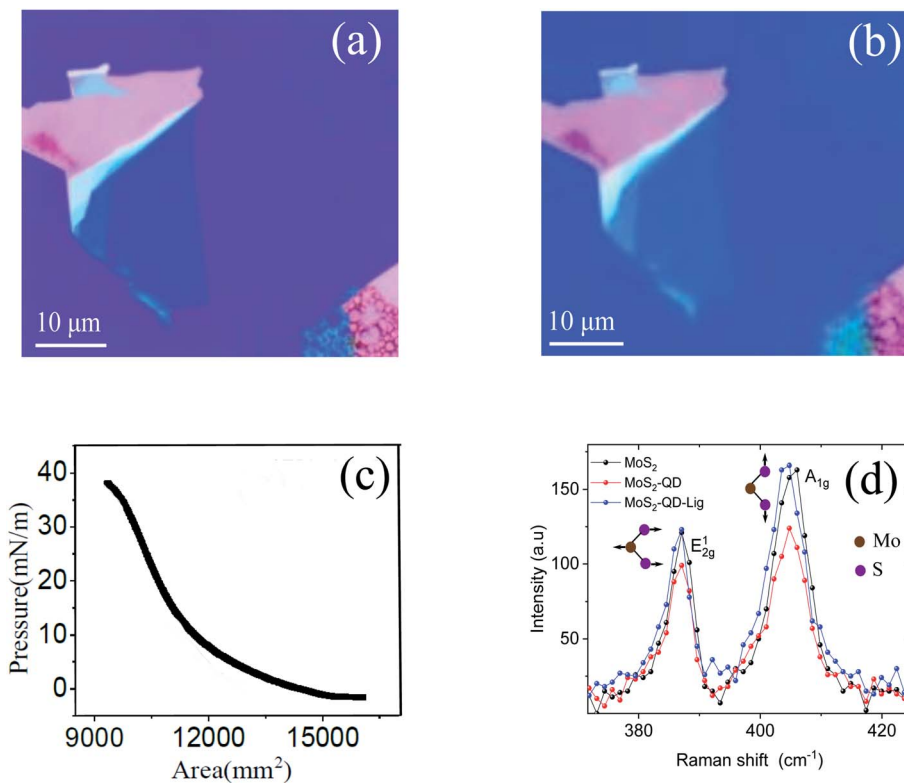


Fig. 2 (a) Optical image of monolayer MoS<sub>2</sub>. (b) The optical images of the MoS<sub>2</sub>-QD hetero-structure after transferring the compact monolayer of the QD film using the Langmuir-Blodgett (LB) technique, with the dot-dot separation,  $\delta$  and the MoS<sub>2</sub>-QD separation,  $d$ , being controlled through chemical methods. (c) The surface pressure vs. area (isotherm) curve of LB for the QD monolayer; the film was transferred at a surface pressure of 35 mN m<sup>-1</sup>. (d) The Raman spectra of MoS<sub>2</sub>, MoS<sub>2</sub>-QDs, and MoS<sub>2</sub>-QDs after ligand exchange.

Fig. 3 shows the PL spectra of the QD-MoS<sub>2</sub> hetero-structure. The energy of QDs was at 2.168 eV. The MoS<sub>2</sub> PL spectra consist of two excitonic peaks at  $\sim 1.85$  eV and  $\sim 2$  eV, related to spin-orbit splitting in the valence band.<sup>21,22</sup> The emission spectra of the chosen QD overlap with the absorption spectra of the higher energy exciton peak of MoS<sub>2</sub>. Both the PL intensities of QDs and MoS<sub>2</sub> decrease in the hetero-structure compared to the PL intensity of the individuals on SiO<sub>2</sub>, consistent with previous reports.<sup>1,2</sup> To quantify the quenching we introduce the

quenching factor  $Q$  defined as  $Q = I_{\text{SiO}_2}/I_{\text{MoS}_2}$ , where  $I_{\text{SiO}_2}$  is the intensity of QDs on SiO<sub>2</sub>, and  $I_{\text{MoS}_2}$  is the intensity of QDs on MoS<sub>2</sub>. When  $d$  is  $\sim 2$  nm, the value of  $Q$  is  $\sim 2.12 \pm 0.05$ . Further the QD energy is blue shifted from 2.168 eV to 2.182 eV which is due to the coupling in the hetero-structure.<sup>4</sup> After ligand exchange, the distance between MoS<sub>2</sub> and QD reduces to  $\sim 0.3$  nm, and the value of  $Q$  becomes  $1.42 \pm 0.01$ . It can be noted that the PL maxima significantly red shift to 2.091 eV and 2.069 eV on SiO<sub>2</sub> and MoS<sub>2</sub>, respectively (Table 1). The full width

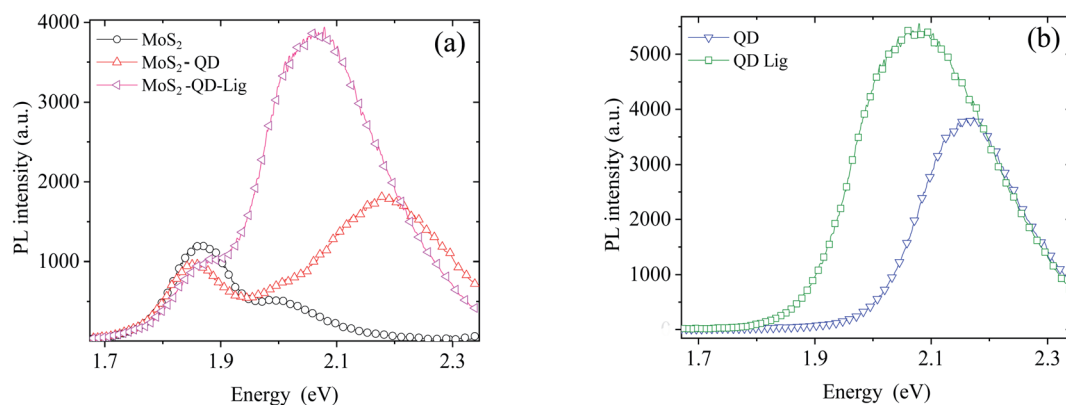


Fig. 3 PL data of (a) the QD-MoS<sub>2</sub> monolayer hetero-structure before and after ligand exchange while (b) shows the same on SiO<sub>2</sub> before and after ligand exchange.



**Table 1** QD PL spectra fitting parameters like center, FWHM, and maxima corresponding to the data in Fig. 3. Detailed fitting is available in Section 3 of the ESI

System	Centre (eV)	FWHM (meV)	Intensity (a.u)
QD	2.168 ± 0.002	203 ± 6	3766 ± 17
QD-Lig	2.091 ± 0.004	263 ± 9	5501 ± 12
MoS <sub>2</sub> -QD	2.182 ± 0.001	210 ± 4	1770 ± 36
MoS <sub>2</sub> -QD-Lig	2.069 ± 0.004	218 ± 2	3847 ± 27

at half maximum (FWHM) of the QD monolayer on SiO<sub>2</sub> is increased from 203 meV to 263 meV after ligand exchange; this broadening and red shift indicate that the coupling between QDs in the highly compact itself has increased due to reduction in  $\delta$ .<sup>23–25</sup> The details are shown in Table 1. Thus the analysis of PL spectra already reveals significant reduction in expected QD PL quenching. However, we do not have complete information about the energy or charge transfer processes from these PL spectra which are known to occur between these 0D–2D hybrid materials. For this we next discuss the TRPL data collected on the same systems as discussed above.

Fig. 4 shows the TRPL data of the QD in the QD–MoS<sub>2</sub> monolayer hetero-structure. All data can be fitted with bi-exponential functions. For the QD monolayer before ligand exchange on SiO<sub>2</sub> the longer lifetime (amplitude)  $\tau_1$  is 5.8 ns

(30%), while the shorter lifetime (amplitude)  $\tau_2$  is 0.9 ns (70%) with the total weighted average lifetime  $\tau$  of 4.5 ns. On MoS<sub>2</sub> these values become  $\tau_1 = 4.4$  ns (17%),  $\tau_2 = 0.7$  ns (83%), and  $\tau = 2.8$  ns, respectively. This decrease in lifetime along with the decrease in PL intensity of QD PL on MoS<sub>2</sub> indicates non-radiative energy transfer from the QD monolayer to MoS<sub>2</sub>. After ligand exchange and a consequent reduction of  $\delta$  and  $d$ ,  $\tau$  on SiO<sub>2</sub> itself decreases to 1.4 ns with  $\tau_1 = 3.0$  ns (10%), and  $\tau_2 = 0.5$  ns (90%). This indicates that the coupling between QDs has significant influence on the lifetime. The lifetime further decreases on MoS<sub>2</sub> after ligand exchange to 0.9 ns with  $\tau_1 = 2.6$  ns (5%), and  $\tau_2 = 0.3$  ns (95%). This decrease indicates the enhanced nonradiative decay rate of the QD monolayer in the hetero-structure after the ligand exchange. Table 2 shows the lifetime details of QDs in the hetero-structure. The longer lifetime is usually associated with the intrinsic decay of the QDs while the shorter lifetime can be associated with the interaction between QDs or with the surrounding environment.<sup>26–28</sup> So the shorter lifetime and its amplitude will be very sensitive to the changes in the environment.

Two major non-radiative processes have been suggested to occur in such 0D–2D hybrids<sup>29</sup> – Förster resonance energy transfer (FRET) and charge transfer (CT). The nonradiative energy transfer rate,  $\Gamma_{\text{FRET}}$ , for emitters on 2D materials like graphene and MoS<sub>2</sub>, is related to the distance,  $d$ , as follows,<sup>2,29</sup>

$$\Gamma_{\text{FRET}} \sim \frac{1}{d^4} \int_0^\infty \alpha(E)g(E)E^4 dE \quad (1)$$

where  $\alpha(E)$  is the absorption profile of MoS<sub>2</sub>, and  $g(E)$  is the emission profile of the QDs. It is clear from eqn (1) that  $\Gamma_{\text{FRET}}$  is expected to increase significantly with decreasing  $d$  and hence a strong enhancement in  $\Gamma_{\text{FRET}}$  is expected in our systems after ligand exchange. Moreover, the broadening of the QD PL spectra along with significant red shift after ligand exchange could enhance the overlap with the MoS<sub>2</sub> absorption spectra. This is also expected to further enhance  $\Gamma_{\text{FRET}}$  in the ligand exchanged system leading to stronger emission quenching. However, this is not observed in our PL measurements as discussed earlier.

While there are several methods to estimate  $\Gamma_{\text{FRET}}$  we have utilized a method which combines information from both the PL and TRPL measurements following<sup>2</sup>

$$I_{\text{QD}} \sim \frac{\Gamma_r}{\Gamma_r + \Gamma_{\text{nr}}} \quad (2)$$

$$I_{\text{MoS}_2\text{-QD}} \sim \frac{\Gamma_r}{\Gamma_r + \Gamma_{\text{nr}} + \Gamma_{\text{FRET}}} \quad (3)$$

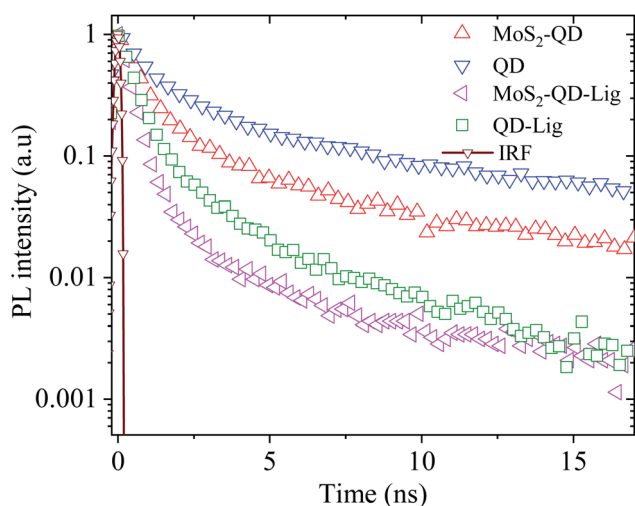


**Fig. 4** TRPL data of the QD–MoS<sub>2</sub> monolayer hetero-structure along with the instrument response function (IRF). All data were fitted with bi-exponential functions as discussed in the ESI.†

**Table 2** The lifetime of QDs in different cases.  $\tau$  is the total weighted average lifetime. Longer and shorter lifetimes are the extracted lifetimes with corresponding contributions in brackets using the bi-exponential fitting

System	Longer lifetime $\tau_1$ (ns)	Shorter lifetime $\tau_2$ (ns)	$\tau$ (ns)
QD	5.8 ± 0.04 (30 ± 2.0%)	0.9 ± 0.04 (70 ± 3.0%)	4.56 ± 0.05
QD-Lig	3.0 ± 0.04 (10 ± 1.0%)	0.5 ± 0.03 (90 ± 1.5%)	1.48 ± 0.01
MoS <sub>2</sub> -QD	4.4 ± 0.05 (17 ± 1.6%)	0.7 ± 0.03 (83 ± 2.0%)	2.76 ± 0.07
MoS <sub>2</sub> -QD-Lig	2.6 ± 0.05 (5 ± 0.5%)	0.3 ± 0.03 (95 ± 1.9%)	0.94 ± 0.11



From the above expressions and using  $1/(I_r + I_{nr}) = \tau_{\text{QD}}$  we get

$$I_{\text{FRET}} = \frac{Q - 1}{\tau_{\text{QD}}} \quad (4)$$

For the TOPO capped QD monolayers, using the value  $Q = 2.12 \pm 0.05$  for longer capped QDs, from the above equation we get  $I_{\text{FRET}} = (2.4 \pm 0.08) \times 10^8 \text{ s}^{-1}$ . Similarly after ligand exchange, using the value  $Q = 1.43 \pm 0.01$  we get  $I_{\text{FRET}} = (2.8 \pm 0.04) \times 10^8 \text{ s}^{-1}$ .

This slight increase in  $I_{\text{FRET}}$  is due to the decrease in  $d$  and the increase in the spectral overlap after ligand exchange. But, as discussed in eqn (1),  $I_{\text{FRET}}$  varies, as  $1/d^4$  according to eqn (1). The center to center distance is calculated from the AFM data (see ESI Fig. S7†) of the QD film by taking the radius of QDs which is  $\sim 3.5$  nm before ligand exchange and  $\sim 2$  nm after ligand exchange with half the  $\text{MoS}_2$  thickness (0.3 nm) being added to these values. The ratio of  $1/d^4$  after and before ligand exchange is  $\sim 7.4$ . Also the increase in the spectral overlap should further increase the FRET rate in the system. However the ratio of  $I_{\text{FRET}}$  after and before ligand exchange is only  $\sim 1.1$ , which suggests that FRET is not the dominant energy transfer process in our hetero-structures. This is surprising given the spectral overlap.

It is well known that there are several conditions which need to be satisfied for FRET to take place between emitters and 2D semiconductors. Two of the main factors are spectral overlap (absorption of  $\text{MoS}_2$  and emission of QDs) and small separation. However, another key factor is related to the kinetics of energy transfer. This involves comparison of the lifetime,  $\tau$ , of the QD and  $(I_{\text{FRET}})^{-1}$ . Basically,  $\tau > (I_{\text{FRET}})^{-1}$  for FRET to be dominant. It is to be noted that  $\tau$ , for our case, has two components,  $\tau_1$  and  $\tau_2$  (Table 2). As mentioned earlier, the longer lifetime,  $\tau_1$ , is the intrinsic excitonic decay while the shorter one,  $\tau_2$ , is due to the QD–QD interaction which is dominant in our compact QD monolayer films. In fact, even for pristine QD films the weight factor for  $\tau_2$  is  $\sim 70\%$  and this becomes even more dominant upon adding additional decay channels due to interactions with  $\text{MoS}_2$  or even upon ligand exchange on  $\text{SiO}_2$  leading to much shorter QD–QD lateral separation and hence even stronger interactions. Clearly, in our compact QD monolayer films  $\tau(\tau_2) < (I_{\text{FRET}})^{-1}$ . While this relationship might also hold for  $\tau_1$  it is definitely valid for  $\tau_2$ , which, in any case, is the dominant lifetime component. This suggests that there are alternative processes which lead to enhancement of decay rate.

However, since our QDs are core only it is possible that other non-radiative processes can exist, especially charge transfer (CT), as has been also suggested to occur in these systems.<sup>11,30,31</sup> Some indication of the presence of CT is also revealed from analysis of the PL data of  $\text{MoS}_2$ . For example, if we consider the ratio  $I_{\text{trion}}/I_{\text{exciton}}$  for  $\text{MoS}_2$  with the TOPO capped QD monolayer on top we find it to be 1.18. We observe an increase in this ratio from 1.18 to 2.08 after ligand exchange treatment of QDs on  $\text{MoS}_2$  suggesting an increase in CT. However, we did not observe a significant change in the  $\text{MoS}_2$  PL intensity suggesting that

other, possibly, radiative processes might be in operation in the hetero-structures. Nevertheless, if we consider that the CT is present, the CT rate can be estimated using the expression:<sup>11</sup>

$$I_{\text{CT}} = \frac{1}{\tau_{\text{MoS}_2\text{-QD}}} - \frac{1}{\tau_{\text{QD}}}, \quad (5)$$

where  $I_{\text{CT}}$  is the CT rate,  $\tau_{\text{MoS}_2\text{-QD}}$  is the total average lifetime of QDs on  $\text{MoS}_2$ , and  $\tau_{\text{QD}}$  is the total average lifetime of QDs on  $\text{SiO}_2$ . We find that before ligand exchange this rate is  $(1.4 \pm 0.2) \times 10^8 \text{ s}^{-1}$  while after ligand exchange this increases to  $(3.9 \pm 0.07) \times 10^8 \text{ s}^{-1}$ . These values are also consistent with enhanced CT in our system after ligand exchange as predicted by the Marcus theory. Conventionally the charge transfer rate increases exponentially with decreasing the distance. The ratio of CT after and before ligand exchange is expected to be  $e_2^{-d}/e_1^{-d} = 4.51$ , however this ratio from the calculated CT rates is 2.7, suggesting that the CT rate might not be following the Marcus theory. However, we now consider the shorter lifetime component,  $\tau_2$ , to compare the CT rates since it is the dominant time scale of relaxation of PL and is also most sensitive to the QD interactions with its environment as discussed earlier. The calculated CT rate from the above expression for  $\tau_2$  is  $(3.2 \pm 0.1) \times 10^8 \text{ s}^{-1}$  and  $(1.3 \pm 0.2) \times 10^9 \text{ s}^{-1}$  before and after ligand exchange respectively. The ratio of CT rates after and before ligand exchange turns out to be 4.16, which is close to  $e_2^{-d}/e_1^{-d}$ . This suggests that the CT process is the dominant non-radiative process (and not FRET) in our hybrid structures and the  $d$  dependence of  $I_{\text{CT}}$  is reasonably consistent with the exponential  $d$  dependence predicted by the Marcus theory, as seen earlier.<sup>11</sup> However, this does not explain the observed reduction in PL quenching of QDs after ligand exchange on  $\text{MoS}_2$ .

We now consider the effect of resonant radiative energy transfer from the QD to  $\text{MoS}_2$  due to the spectral overlap between the QD and B exciton. In order to understand this possible mechanism better we carefully fitted the PL spectra with the combination of Lorentzian and Gaussian peak functions. It is to be noted that (ESI Fig. S2†) pure  $\text{MoS}_2$  PL spectra can be well modeled with 3 Lorentzians corresponding to the A exciton and trion and B exciton. On the other hand the QD PL on  $\text{SiO}_2$  which shows extrinsic broadening due to size dispersity and thermal effects can be well fitted with a single Gaussian peak fitting function (ESI Fig. S3†). Fig. 5(a) shows the cumulative fit of the full PL spectrum including that of  $\text{MoS}_2$  and QDs and also displays the individual fits to the A trion, exciton and B exciton components as well as that due to the QD peak for the TOPO capped QDs on  $\text{MoS}_2$ , using 3 Lorentzians ( $\text{MoS}_2$ ) and 1 Gaussian (QD). It can be seen clearly that the intensity of the trion component is higher than that of A and B exciton components. Fig. 5(b) on the other hand shows the same fitted components, as in Fig. 5(a), corresponding to the system after ligand exchange. However, we could only fit the  $\text{MoS}_2$ –QD spectra satisfactorily with two Lorentzians (A exciton and trion) and two Gaussians (B exciton and QD). It is clearly observed that the B exciton intensity has increased compared to the other components on the A exciton as well as the QDs. The  $I_{\text{A exciton}}/I_{\text{B exciton}}$  is decreased from 3.23 to 1.24 after transferring QDs onto  $\text{MoS}_2$ . This suggests that there is energy transfer between the



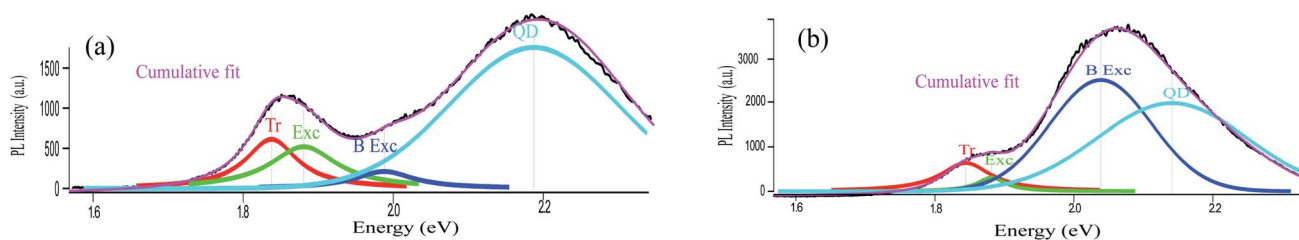


Fig. 5 PL data fitting for the QD–MoS<sub>2</sub> monolayer hetero-structure before and after ligand exchange: (a) fitting before ligand exchange shows that the intensity of B excitons is lower than that of the QD, A exciton and trion. (b) After ligand exchange the fit shows that the intensity of B excitons is higher than that of the QD, A trion and exciton.

QD and B exciton although we do not observe a similar decrease in QD PL intensity. In fact the QD component of the PL spectrum cannot be well fitted with a single Gaussian (ESI Fig. S4†) as well indicating a strong overlap between the B exciton (2D) and the QD exciton (0D). Thus coupled with the observation that after ligand exchange the PL spectra can be fitted better with 2 Lorentzians (MoS<sub>2</sub> A) and 2 Gaussians (QD + B), it is suggested that a hybrid state (0D–2D) in this resonantly coupled system is, possibly, formed with the B exciton and coupled QDs exchanging energy coherently such that simultaneous enhancement of B exciton intensity and strong suppression of QD PL quenching take place.

## 4 Conclusions

In summary, we control the emission efficiency of core QDs in the monolayers of the MoS<sub>2</sub>–QD hetero-structure using ligand exchange treatment. At larger separations we observe quenching of QD PL due to non-radiative processes, at smaller separations we observe enhanced emission from QDs on MoS<sub>2</sub> as compared to the larger *d* despite the presence of significant non-radiative charge transfer. Interestingly, at small separations, we see evidence of strong dot-dot interactions and a significant red shift of QD PL maxima which enhances spectral overlap with the absorption of B excitons of MoS<sub>2</sub>. Despite the increased probability of non-radiative resonant energy transfer to MoS<sub>2</sub> from QDs due to increased spectral overlap as well as that due to enhanced CT we find that the quenching of the PL of QDs is significantly reduced as compared to longer separations as well as to what would be expected from the non-radiative processes. Concurrent with this reduced QD PL quenching, the intensity of the B exciton of MoS<sub>2</sub> increases significantly suggesting the possibility of coherent and resonant radiative energy exchange between the 0D excitons in QDs and the 2D B exciton in MoS<sub>2</sub>. We observe that the ligand exchange is an effective technique to tune the nonradiative decay channels in the 0D–2D hetero-structure. Our study reveals interesting nanoscale light–matter interaction effects which can suppress the conventional quenching of QDs leading to potential applications of these nanoscale devices in photonics.

## Conflicts of interest

There are no conflicts to declare.

## Acknowledgements

HLP thanks CSIR-UGC for financial support. The authors thank DST nanomission for funding. The authors thank SERB, India for funding. HLP thanks Mangesh and Puspender for help in using Igor software.

## Notes and references

- 1 A. Raja, A. Montoya-Castillo, J. Zultak, X.-X. Zhang, Z. Ye, C. Roquelet, D. A. Chenet, A. M. Van Der Zande, P. Huang, S. Jockusch and T. F. Heinz, *Nano Lett.*, 2016, **16**, 2328–2333.
- 2 D. Prasai, A. R. Klots, A. Newaz, J. S. Niezgodna, N. J. Orfield, C. A. Escobar, A. Wynn, A. Efimov, G. K. Jennings and S. J. Rosenthal, *Nano Lett.*, 2015, **15**, 4374–4380.
- 3 H. Zang, P. K. Routh, Y. Huang, J.-S. Chen, E. Sutter, P. Sutter and M. Cotlet, *ACS Nano*, 2016, **10**, 4790–4796.
- 4 K. M. Goodfellow, C. Chakraborty, K. Sowers, P. Waduge, M. Wanunu, T. Krauss, K. Driscoll and A. N. Vamivakas, *Appl. Phys. Lett.*, 2016, **108**, 021101.
- 5 S. Sampat, T. Guo, K. Zhang, J. A. Robinson, Y. Ghosh, K. P. Acharya, H. Htoon, J. A. Hollingsworth, Y. N. Gartstein and A. V. Malko, *ACS Photonics*, 2016, **3**, 708–715.
- 6 A. Boulesbaa, K. Wang, M. Mahjouri-Samani, M. Tian, A. A. Poretzky, I. Ivanov, C. M. Rouleau, K. Xiao, B. G. Sumpter and D. B. Geohegan, *J. Am. Chem. Soc.*, 2016, **138**, 14713–14719.
- 7 P. Rivera, J. R. Schaibley, A. M. Jones, J. S. Ross, S. Wu, G. Aivazian, P. Klement, K. Seyler, G. Clark and N. J. Ghimire, *Nat. Commun.*, 2015, **6**, 1–6.
- 8 M. Okada, A. Kutana, Y. Kureishi, Y. Kobayashi, Y. Saito, T. Saito, K. Watanabe, T. Taniguchi, S. Gupta and Y. Miyata, *ACS Nano*, 2018, **12**, 2498–2505.
- 9 H. L. Pradeepa, P. Mondal, A. Bid and J. K. Basu, *ACS Appl. Nano Mater.*, 2020, **3**, 641–647.
- 10 J. S. Ross, S. Wu, H. Yu, N. J. Ghimire, A. M. Jones, G. Aivazian, J. Yan, D. G. Mandrus, D. Xiao and W. Yao, *Nat. Commun.*, 2013, **4**, 1474.
- 11 J.-S. Chen, M. Li, Q. Wu, E. Fron, X. Tong and M. Cotlet, *ACS Nano*, 2019, **13**, 8461–8468.
- 12 S. Zhang, X. Wang, Y. Chen, G. Wu, Y. Tang, L. Zhu, H. Wang, W. Jiang, L. Sun and T. Lin, *ACS Appl. Mater. Interfaces*, 2019, **11**(26), 23667–23672.



- 13 M. Li, J.-S. Chen, P. K. Routh, P. Zahl, C.-Y. Nam and M. Cotlet, *Adv. Funct. Mater.*, 2018, **28**, 1707558.
- 14 D. Kufer, I. Nikitskiy, T. Lasanta, G. Navickaite, F. H. Koppens and G. Konstantatos, *Adv. Mater.*, 2015, **27**, 176–180.
- 15 H. Chen, H. Liu, Z. Zhang, K. Hu and X. Fang, *Adv. Mater.*, 2016, **28**, 403–433.
- 16 L. Qu and X. Peng, *J. Am. Chem. Soc.*, 2002, **124**, 2049–2055.
- 17 C. de Mello Donega, S. G. Hickey, S. F. Wuister, D. Vanmaekelbergh and A. Meijerink, *J. Phys. Chem. B*, 2003, **107**, 489–496.
- 18 J. R. Heath, C. M. Knobler and D. V. Leff, *J. Phys. Chem. B*, 1997, **101**, 189–197.
- 19 M. Haridas, J. K. Basu, A. Tiwari and M. Venkatapathi, *J. Appl. Phys.*, 2013, **114**, 064305.
- 20 H. J. Yun, T. Paik, M. E. Edley, J. B. Baxter and C. B. Murray, *ACS Appl. Mater. Interfaces*, 2014, **6**, 3721–3728.
- 21 A. Kormányos, G. Burkard, M. Gmitra, J. Fabian, V. Zólyomi, N. D. Drummond and V. Fal'ko, *2D Mater.*, 2015, **2**, 022001.
- 22 K. F. Mak, K. He, C. Lee, G. H. Lee, J. Hone, T. F. Heinz and J. Shan, *Nat. Mater.*, 2013, **12**, 207.
- 23 J.-H. Choi, A. T. Fafarman, S. J. Oh, D.-K. Ko, D. K. Kim, B. T. Diroll, S. Muramoto, J. G. Gillen, C. B. Murray and C. R. Kagan, *Nano Lett.*, 2012, **12**, 2631–2638.
- 24 C. R. Kagan and C. B. Murray, *Nat. Nanotechnol.*, 2015, **10**, 1013.
- 25 J.-S. Lee, M. V. Kovalenko, J. Huang, D. S. Chung and D. V. Talapin, *Nat. Nanotechnol.*, 2011, **6**, 348.
- 26 W.-S. Chae, T. D. T. Ung and Q. L. Nguyen, *Adv. Nat. Sci.: Nanosci. Nanotechnol.*, 2013, **4**, 045009.
- 27 M. Praveena, T. Phanindra Sai, R. Dutta, A. Ghosh and J. K. Basu, *ACS Photonics*, 2017, **4**, 1967–1973.
- 28 R. Dutta, K. Jain, M. Venkatapathi and J. K. Basu, *Phys. Rev. B*, 2019, **100**, 155413.
- 29 B. Guzelturk and H. V. Demir, *Adv. Funct. Mater.*, 2016, **26**, 8158–8177.
- 30 H. Wu, Z. Kang, Z. Zhang, Z. Zhang, H. Si, Q. Liao, S. Zhang, J. Wu, X. Zhang and Y. Zhang, *Adv. Funct. Mater.*, 2018, **28**, 1802015.
- 31 A. J. Goodman, N. S. Dahod and W. A. Tisdale, *J. Phys. Chem. Lett.*, 2018, **9**, 4227–4232.

